



Optical interactions and white light emission in Eu:Y₂O₃/YAG:Ce nanophosphor

Rashmi¹ · Y. Dwivedi¹

Received: 29 May 2019 / Accepted: 15 July 2019 / Published online: 23 July 2019
© Springer-Verlag GmbH Germany, part of Springer Nature 2019

Abstract

Detailed structural and optical analysis of composite nanophosphor (Eu:Y₂O₃)/(Y₃Al₅O₁₂:Ce) was presented and compared with Eu:Y₂O₃ and Y₃Al₅O₁₂:Ce (YAG:Ce) nanophosphors. The nanophosphor was synthesized by adopting the combustion synthesis route subsequently co-precipitation method. The detail structural and spectroscopic characterizations were carried out using different techniques including XRD, TEM, SEM, FTIR, and PL. The XRD analysis indicates the formation of tiny crystals (12–24 nm) which was supported by SEM and TEM images. FTIR absorption spectra confirm the coordination between Eu:Y₂O₃ and YAG:Ce phosphors. The laser excitations by 405 nm and 450 nm stimulate sharp and intense red emission in Eu:Y₂O₃ and a broad asymmetric green–yellow emission in YAG:Ce nanophosphor. The Eu:Y₂O₃/YAG:Ce composite nanophosphor yields combinatorial emissions of Ce³⁺ and Eu³⁺ ions; though, the intensity was found to be modified due to the interaction between the ions doped in nanophosphors. The emission of Eu:Y₂O₃/YAG:Ce was extended in the red region (670 nm). Detailed emission properties were investigated on 342, 381, 405, 450, and 464 nm excitations, in addition to dual-beam excitations (405 nm + 450 nm). The energy transfer from Ce³⁺ → Eu³⁺ ions was established on the basis of emission intensity improvement in the Eu³⁺ ion at the cost of the emission intensity of Ce³⁺ ion and appearance of Eu³⁺ ion emission while exciting Ce³⁺ ion. The color perception of the nanophosphor was observed to be significantly modified at different excitation wavelengths, and laser power as reflected by CIE coordinates. The detail photophysics of the observed modification is well explained.

1 Introduction

A plethora of research on lanthanide-doped Y₃Al₅O₁₂ nanophosphor is well employed for the realization of polychromatic emission which is webbed over visible spectral region. Trivalent lanthanide ions are known to yields sharp primary colors (red, green, and blue), while the divalent lanthanide ions are reported to emit broad band suitable to stimulate white light of desired perception. The white color perception can be precisely attuned by an adequate selection of the host, excitation wavelength, doping concentrations, etc. Cerium-activated yttrium aluminum garnet [1, 2] has

been proved to be boon for superior luminance performance and widely utilized for the various applications including X-ray [3] and γ -ray detectors [4], LED [5], thermographic phosphor [6], etc. YAG:Ce nanophosphor possess excellent characteristics, for example, high thermal conductivity [7] (10–14 W m⁻¹ K⁻¹), thermochemical stability, high quantum efficiency, [8–13], and fast spontaneous emission rate, etc. Similar to YAG:Ce nanophosphor, another important inorganic oxide material is Eu:Y₂O₃, which is known for bright and sharp red emission and prolonged relaxation time. Due to these properties, Eu:Y₂O₃ are often used in sensors [14], cathode ray tube display, lightening applications [15, 16], etc. The optical properties of Eu may vary as the Eu ion possesses 3+ and 2+ valance states. It has been observed that under suitable ambient reaction parameters, synthesis temperature, etc., Eu³⁺ ion may convert to Eu²⁺ ion. This conversion can be either partial or complete. Eu²⁺ ion emits broad and bright emission in the blue region due to the transition from the 5d → 4f [17–19]. The presence of broad blue emission rather than red emission limited the scope of Eu³⁺ ion application, while Ce³⁺ ions is codoped

Electronic supplementary material The online version of this article (<https://doi.org/10.1007/s00339-019-2830-3>) contains supplementary material, which is available to authorized users.

✉ Y. Dwivedi
yashjidwivedi@nitkkr.ac.in

¹ Department of Physics, National Institute of Technology Kurukshetra, Haryana 136119, India

in the same lattice [20, 21]. One of the interesting solutions of the problem would be the design of the composite material which brings YAG:Ce and Eu-doped nanophosphor in suitable closed proximity. These materials can facilitate the energy transfer from sensitizer to the activator, due to the successive photon absorption and energy transfer steps, on account of their partial overlapping energy levels. Over the past few years, a lot of core-shell-structured materials and composites were successively studied, such as $\text{Al}_2\text{O}_3/\text{YAG:Ce}$ phosphor [22], $\text{SiO}_2/\text{Y}_2\text{O}_3:\text{Eu}$ [23], and YAG:Ce/YAG:Cr [24].

In the present article, efforts were made to synthesize composite material of YAG:Ce and $\text{Eu:Y}_2\text{O}_3$ nanophosphors. As Eu ion is not in the same lattice of Ce^{3+} ion, it retains its +3 valence state. Also, efforts have been made to tune the white perception in reddish region via energy transfer from YAG:Ce matrix to $\text{Eu:Y}_2\text{O}_3$. The developed material is reported to tune the overall photoluminescent properties.

2 Synthesis and characterizations

2.1 Chemicals

For the synthesis of $\text{Eu:Y}_2\text{O}_3/\text{YAG:Ce}$ nanophosphors, following materials were employed: europium oxide [Eu_2O_3] (99.90%), yttrium oxide [Y_2O_3] (99.90%), aluminum nitrate [$\text{Al}(\text{NO}_3)_3 \cdot 9\text{H}_2\text{O}$] (99.90%), cerium chloride [$\text{CeCl}_2 \cdot 7\text{H}_2\text{O}$] (99.99%), glycine [$\text{NH}_2\text{CH}_2\text{COOH}$] (99.99%), ammonia solution (NH_4OH), and hydrochloric acid (HCl), etc. These chemicals were purchased from Sigma-Aldrich Company and were used as received.

2.2 Synthesis

In the present work, $\text{Eu:Y}_2\text{O}_3$, YAG:Ce, and $\text{Eu:Y}_2\text{O}_3/\text{YAG:Ce}$ nanophosphors were synthesized by using the protocol of two different synthesis methods namely co-precipitation [25] and combustion [26, 27]. The bulk solution of yttrium chloride was prepared by dissolving the required amount of Y_2O_3 in concentrate hydrochloric acid (1 M). At the first step, individual aqueous solutions of aluminum nitrate and yttrium chloride were prepared and mixed together in stoichiometric proportion, while rigorous stirring for an hour at room temperature. Later on, the desired amount of cerium chloride solution was added in the above mixture drop-by-drop while stirring to maintain the Ce^{3+} ion molar concentrations 01%. Finally, the required solution of fuel (glycine) was added drop-wise to the solution and well stirred at least for an hour to achieve homogeneous mixing. The oxidizer-to-fuel molar ratio was taken to be 01:1.17. The solution obtained was stirred for the next 2 h at elevated

temperature (313 K) in order to prepare gel. The obtained gel was combusted at 973 K in a platinum crucible. As a result of combustion, the exothermic reaction starts, leading to the fast removal of gases and consequently, bubble formation takes place resulting in the expansion of the gel. The fast removal of gases results in a dry fluffy voluminous light-brown mass. Samples were annealed at the pre-optimized temperature, i.e., 1373 K and annealing time duration 5 h (for emission intensity at 530 nm) in order to obtain the single-phase YAG crystalline material.

$\text{Eu:Y}_2\text{O}_3/\text{YAG:Ce}$ nanophosphor was synthesized by co-precipitation. Herein, the bulk solution of yttrium chloride and europium chloride was prepared by dissolving the required amount of Y_2O_3 and Eu_2O_3 in concentrate hydrochloric acid (01 M). Later on, the individual aqueous solution of europium chloride and yttrium chloride was prepared and mixed together in stoichiometric proportion. The mixture was kept for rigorous stirring for 30 min at room temperature. Later on, the desired amount of synthesized YAG:Ce was well dispersed in 05 ml of distilled water and ultrasonicated for 15 min to reduce the agglomeration, if any. This solution was added in the mixture of metal salts drop-by-drop while stirring at least for an hour to achieve homogeneous mixing. Finally, the required amount of ammonia solution was added drop-wise while stirring. Once the precipitation occurs, the obtained solution was kept undisturbed to settle down for the overnight. The obtained precipitated solution was dried at 50 °C in an electric oven for 12 h. The resultant yellowish-white powder was annealed at 1173 K temperature for 3 h. The final product obtained was used for further analysis. To explore the mutual effect of YAG:Ce and $\text{Eu:Y}_2\text{O}_3$ while present in the close proximity, samples of different weight ratios 01:03 and 01:06 of YAG:Ce and $\text{Eu:Y}_2\text{O}_3$ were synthesized. Herein, the notation 3EY and 6EY were used for the 01:03 and 01:06 weight ratios of (YAG:Ce):(Eu:Y₂O₃) nanophosphor, respectively.

2.3 Characterizations

The structural characterization was performed using powder X-ray diffraction (XRD) recorded on a Rigaku mini-diffractometer using graphite-filtered Cu-K_α radiation ($\lambda = 1.5406 \text{ \AA}$). The operating voltage was 40 kV (100 mA) with a scanning rate of $02^\circ \text{ min}^{-1}$ (in the range of 10° – 80° angle). Electron microscopic images were captured on the scanning electron microscope (JSM-6390LV) at an acceleration voltage of 10 kV. Transmission electron microscope (FEI Tecnai G² F20) operated at 200 kV was used to estimate the size and the selected area diffraction pattern. Diffused light scattering (DLS) characterization was performed on Litesizer™ instrument. Laser emitting at 658 nm wavelength (power 40 mW) was used as a light source with the measuring range extended over 0.3–10 μm (particle diameter) at

measurement angles 175°. Absorption spectra of the samples were monitored on UV–visible absorption spectrophotometer (T90+ double-beam scanning) in the wavelength range 200–900 nm. Fourier transformed infrared (FTIR) absorption spectra of the samples were recorded, in the range of wave number 400–4000 cm⁻¹, on Carry eclipse 6300 machine using attenuated total reflectance (ATR) technique. Photoluminescence (PL) and photo-excitation (PLE) spectra were measured using a fluorescence setup: model number RF-530 (Shimadzu, Japan) in the range 200–800 nm. The PL spectra of the samples were also monitored using 405 nm and 450 nm laser diodes as excitation sources, a charge-coupled detector (Avantes Netherland), and optical fibers assembly. Radiative decay curves were recorded by DeltaFlex™ modular fluorescence lifetime system of company Horiba scientific (USA) having time resolution ± 1 ns. The decay curves were recorded using lasers, emitting at 405 nm and 450 nm wavelengths, and the lifetime was estimated by fitting as exponential function to the decay curves. The Commission Internationale de l’Eclairage (CIE) coordinates and the correlated color temperature (CCT) values were calculated using expressions in Ref. [28].

3 Results and discussion

3.1 Nanostructural analysis

The identification and purity of the phases precipitated in the prepared samples were monitored using powder X-ray diffraction (XRD) technique and displayed in Fig. 1. The diffraction patterns of Eu:Y₂O₃ nanophosphor annealed at 1173 K for 03 h, and YAG:Ce nanophosphor annealed at 1373 K for 5 h, exhibiting sharp diffraction peaks. These peaks correspond to the characteristic crystalline planes of Y₂O₃ and Y₃Al₅O₁₂ (YAG) phases, and the crystalline planes were well matched with JCPDS no. 025-1011 (Y₂O₃) [29] and JCPDS no. 072-1853 (Y₃Al₅O₁₂) [30–32] crystalline phases of cubical symmetry. The XRD pattern of synthesized 3EY nanophosphor (annealed at 1173 K/3 h) is an amalgam of the patterns of YAG and Y₂O₃ phases. While comparing the diffraction pattern with their individual constituents, it was observed that some of the diffraction peaks get broadened. The observed broadness in the peak was expected due to the overlapping of some of the crystalline peaks of YAG and Y₂O₃ phases (see Fig. 1). Comparing the patterns of YAG:Ce with the 3EY, it is evident that the diffraction peaks corresponding to the YAG:Ce in 3EY shifted toward higher angle side ($2\theta \sim 01$).

Additionally, the peak broadening of $2\theta \sim 0.3 \pm 0.03$ angle was observed in the 3EY as compared to YAG:Ce sample. On the other hand, the diffraction patterns of the Y₂O₃ sample shows only a slight variation in intensity and the peak

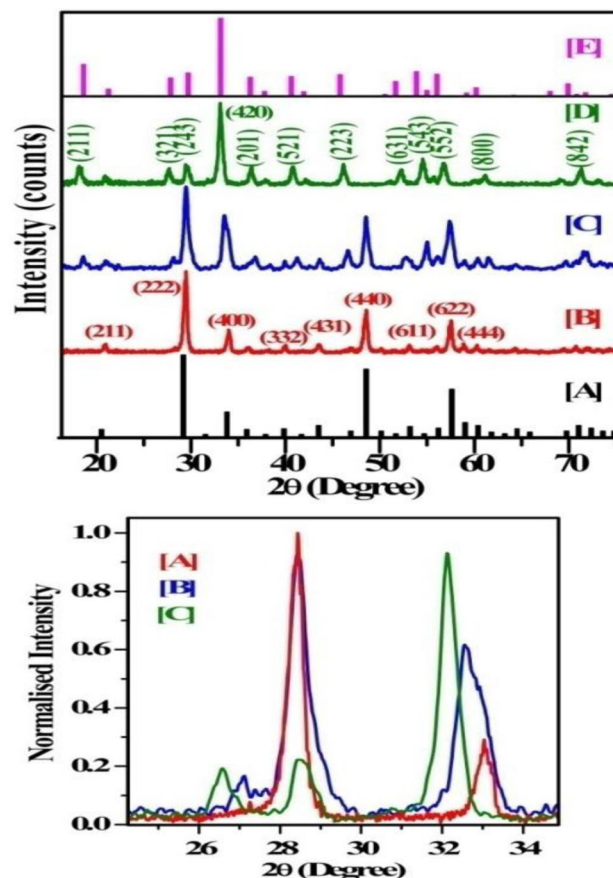


Fig. 1 Up: comparison between the diffraction patterns of the synthesized nanophosphors; reference patterns of Y₂O₃ [A] and YAG [E]; synthesized Eu:Y₂O₃ [B]; 3EY [C]; YAG:Ce [D] nanophosphors. Down: the enlarged portion of the patterns Eu:Y₂O₃ [A], 3EY [B], and YAG:Ce [C] nanophosphors for comparison

position. The obvious slight variation in the peak positions of the YAG phase in 3EY is expected due to the presence of Eu:Y₂O₃. The average crystallite size was estimated using Debye–Scherrer’s relation. The size and strain was estimated for Eu:Y₂O₃, Eu:Y₂O₃/YAG:Ce, and YAG:Ce nanophosphors and found to be 24 nm, 12 nm, and 20 nm; and 0.0054, 0.011, and 0.0065, respectively. Interestingly, the estimated strain, in the 3EY sample, is approximately twice of the pure phase. The calculated lattice parameter of Eu:Y₂O₃ was 10.8 Å which is slightly higher than the value (10.6 Å) of the bulk Y₂O₃ phase; similarly, in the case of YAG nanophosphor, the lattice parameter was found to be 12.4 Å which is slightly higher than the value of bulk YAG (12.0 Å).

The surface morphology of the YAG:Ce and 3EY nanophosphor were characterized by scanning electron microscope (SEM), shown in Fig. 2 and S1. The material surface is appeared to be spongy-like structure, formed due to the assembly of agglomerated particles creating the porous artifact. The nanophosphor network was abundant of pores

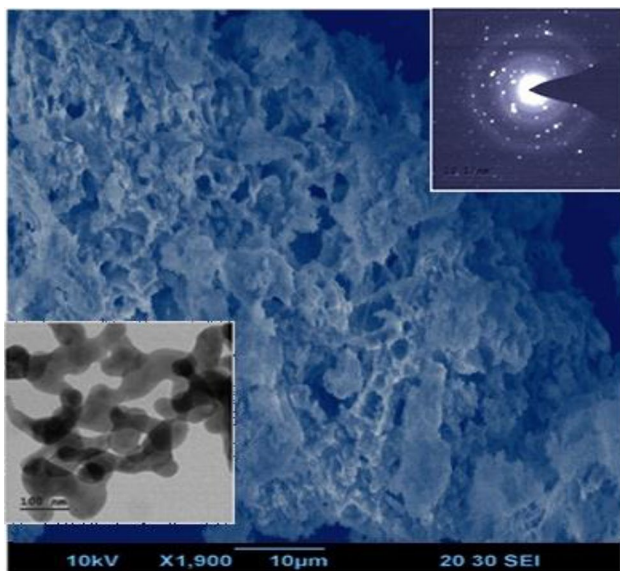


Fig. 2 SEM image of 3EY sample annealed at temperature 1173 K/3 h. (Right: up) selected area diffraction pattern of 3EY sample; (left: down) the TEM image

and voids. The observed network is expected to form due to the high-temperature annealing and consequently fast release of gases. The information about the particle size is not much clear due to the limited resolution of the existing microscope.

TEM image reveals the distribution of randomly distributed particles of spheroidal shape in interconnected chain network. The image shows the overlapping of nanoparticles consequently darken the particles. The selected area electron diffraction (SAED) pattern of 3EY nanophosphor comprises various sharp bright spots that are distributed randomly (Fig. 2). The observed spot reveals the crystalline nature of the sample, though due to the overlapping of the particles the indexing of the spots is difficult. The TEM image of YAG:Ce nanophosphor is shown in Fig. S1.

Attempts were made to analyze the effect of (Eu:Y₂O₃) in presence of the (YAG:Ce nanophosphor) in 3EY sample, using dynamic light scattering (DLS) experiment [33]. In the case of 3EY, the hydrodynamic size was appeared to be enlarged ($\Delta \sim 08\%$) in comparison with YAG:Ce. This slight variation ($\Delta \sim 08\%$) reveals the presence of Eu:Y₂O₃ near the surface of YAG:Ce nanophosphor.

3.2 Reflection analysis

Reflection spectrum of electronic transitions corresponding to the individual constituents and 3EY nanophosphors was compared (see Fig. 3).

In the reflectance spectrum of YAG:Ce sample, at least five asymmetric absorption bands were marked

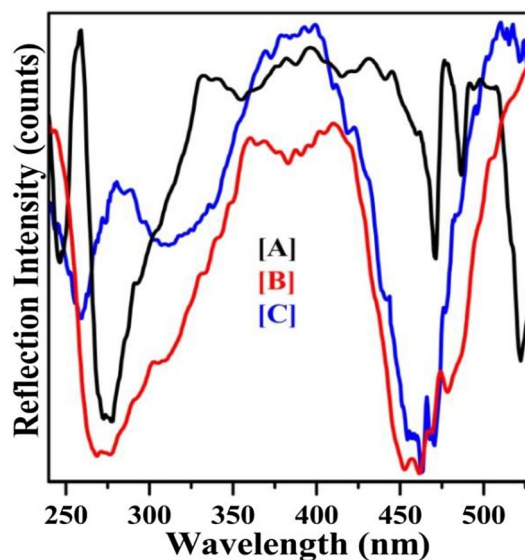


Fig. 3 A comparison between UV-visible normalized reflection spectra of Eu:Y₂O₃ [A]; 3EY [B]; and YAG:Ce [C] nanophosphors

corresponding to the $4f-5d$ transitions [34–36] of the Ce³⁺ ion. The asymmetric band centered at 260 nm is accompanied by a weak band at 235 nm; similarly another asymmetric band centered at 312 nm and shoulder at 330 nm. The most intense and broad reflection band located at 468 nm. Considering the absorption profile of Eu:Y₂O₃ sample, charge transfer bands [37, 38] were observed at 245 nm and 278 nm. The absorption peaks at 466 nm, 487 nm, 532 nm, and 535 nm were observed in the reflectance spectrum of Eu:Y₂O₃ nanophosphor, corresponding to the characteristic transitions ${}^7F_0, {}^7F_1 \rightarrow {}^5D_2$; ${}^7F_0, {}^7F_1 \rightarrow {}^5D_1$ of the Eu³⁺ ion [17, 39], respectively. In the case of 3EY, the absorption bands found were an amalgam of characteristic and charge transfer absorption bands of Eu³⁺ and Ce³⁺ ion. In the 3EY sample, most interestingly, the band at 466 nm, due to the Ce³⁺ ion, shifted ~ 16 nm toward higher energy side. The observed shifting is expected due to the presence of Eu:Y₂O₃ nanophosphor near YAG:Ce nanoparticles surface, as the comparably open-shell structure of $5d$ band (of surface Ce³⁺ ion) is susceptible to the ambience bonding parameters.

3.3 Infrared absorption analysis

To estimate the variation in molecular vibrations, in the presence of Eu:Y₂O₃ and YAG:Ce nanophosphors, infrared absorption spectra of these samples were monitored and compared (Fig. 4). The infrared absorption spectrum of Eu:Y₂O₃ nanophosphor comprise of the characteristic IR bands Y–O bond in Y₂O₃ at 426, 452, 473, 518, and 560 cm⁻¹ [12, 40].

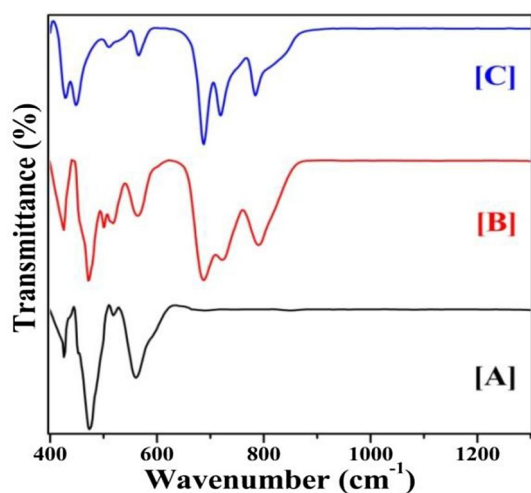


Fig. 4 A comparison between the FTIR transmittance spectra of Eu:Y₂O₃ [A], 3EY [B], and YAG:Ce [C] nanophosphors

In YAG:Ce, absorption bands at 430, 448, 510, 534, and 566 cm⁻¹ represent the characteristic Y–O located at 510, 534, and 566 cm⁻¹ are ascribed due to symmetric and asymmetric stretching of Al–O bond, whereas a band centered at 430 cm⁻¹ band is ascribed due to the Al–O translation (T_0) in octahedral symmetry. Sharp peaks over a broad band at 688, 719, and 784 cm⁻¹ are ascribed due to asymmetric stretching of tetrahedron Al–O vibrations [41–44].

The interaction between Eu:Y₂O₃ and YAG:Ce nanophosphors, in the 3EY may be verified by FTIR absorption spectra. The absorption spectrum of the 3EY sample was comprised of YAG and Y₂O₃ host vibrations. Although, it was noticed that the absorption bands corresponding to YAG host were broadened and shifted toward lower energy side (Fig. 4). The bands located at 501, 520, and 563 cm⁻¹ are ascribed due to the symmetric and asymmetric stretching of Al–O bond, whereas a band centered at 427 cm⁻¹ is shifted from 430 cm⁻¹ as in YAG:Ce which was ascribed due to the translation of Al–O bond. Band centered at 475 cm⁻¹ is attributed due to vibrations of octahedral symmetry of Al–O bond. The sharp peaks 688, 723, and 790 cm⁻¹ were assigned as symmetric and asymmetric stretching vibrations of Al–O bond.

3.4 Photoluminescence analysis

To explore the radiative transition properties of individual constituents of 3EY, photo-excitation and photoluminescence spectra of synthesized samples were monitored. In the case of 01 mol% Eu³⁺-doped Y₂O₃ nanophosphor, various sharp excitation peaks were observed corresponding to the brightest emission line at 615 nm of the Eu³⁺ ion. The excitation peaks were observed at 361, 381, 393, 465, and 531 nm due to the intra-ionic 4*f*–4*f* transitions

[18, 19]. When the same sample was excited with 464 nm, characteristic emission peaks located at 584 nm, 589 nm, 597 nm, 603 nm, 615 nm, 633 nm, 654 nm, and 710 nm were observed. These peaks are attributed to the transitions from excited level ⁵D₀ to various low energy levels ⁷F_{0,1,2,3,4,5} of Eu³⁺ ion [39], respectively. YAG:Ce nanophosphor was reported to yield broad green–yellow emission (centered at 530 nm) band which extend to the red region (up to 620 nm) [3, 27, 35]. The emission, at lower energy, partially overlaps with the bright emission of the Eu³⁺ ion. Photo-excitation spectrum of YAG:Ce nanophosphor for 615 nm (corresponding to Eu³⁺ ion emission) comprises of major two bands at 340 nm and 460 nm, similar to the reflectance emission of the same. In the case of YAG:Ce nanophosphor, when excited with 464 nm, an asymmetric bright green–yellow (centered at 530 nm) band of Ce³⁺ observed. The emission band was originated due to the transitions of excited electrons from the lowest 5*d*:²D_{3/2} state [20, 21]. The comparison between the excitation spectra of YAG:Ce and Eu:Y₂O₃ with 3EY nanophosphor reveals the presence of characteristic peaks corresponding to the Eu³⁺ and Ce³⁺ ion, leading to the significant improvement in the overall absorption of the 3EY nanophosphor in violet–visible regions. On comparing the excitation peak positions of the Ce³⁺ ion (530 nm emission) and Eu³⁺ ion (615 nm emission), interestingly, the excitation peak at 464 nm is well overlapped with the excitation peaks of the Ce³⁺ ions. This indicates the simultaneous excitations of both the doped ions (Ce³⁺ and Eu³⁺) by 464 nm radiations. In the case of 3EY, excitation photons of wavelength 464 nm stimulates emission from both the ionic species (Ce³⁺ and Eu³⁺) leading to the combined emission overlying on each other emission profile. Broad green–yellow emission band attributed to the characteristic emission of Ce³⁺ ion and several sharp emission bands in the red region attributed to the characteristic emission of trivalent Eu³⁺ states were observed (see Fig. 5). The broad emission band of Ce³⁺ ion significantly overlapped with the excitation peak of the Eu³⁺ ion at 532 nm. The prominent overlapping speculates the significant interaction between the constituent nanophosphors of 3EY. Due to this overlapping, a slight reduction in intensity of Ce³⁺ ion emission was observed which indicates the partial absorption of Ce³⁺ ion emission by Eu³⁺ ion. In case of YAG:Ce nanophosphor, the FWHM of the emission profile ($\lambda_{\text{ex}} = 464$ nm) was 86 nm, while in case of 3EY, the FWHM of emission profile for the identical excitation wavelength, gets broadened (by the factor of 11 nm) and observed to be 97 nm. The combined photoluminescence spectrum of the 3EY is observed to extend in the red region up to 670 nm wavelength.

On careful analysis, it was noticed that only a few selected regions remain un-overlapped, corresponding to each of the individual ions (Ce³⁺ and Eu³⁺ ions). For example, the wavelengths 342 nm and 381 nm only excites Ce³⁺ and Eu³⁺ ions,

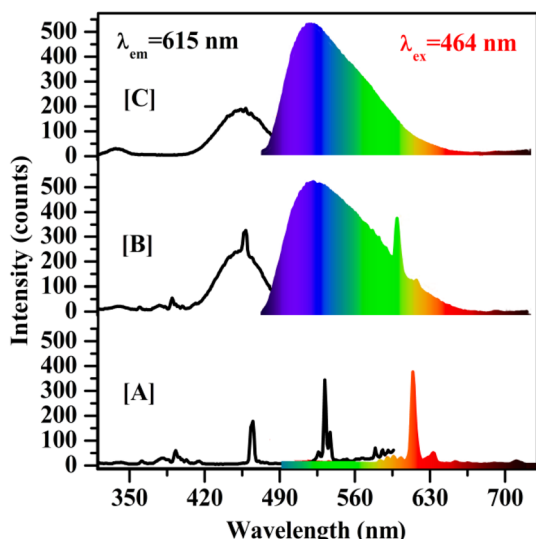


Fig. 5 Excitation and photoluminescence spectra of Eu:Y₂O₃ [A], 3EY [B], and YAG:Ce [C] nanophosphors

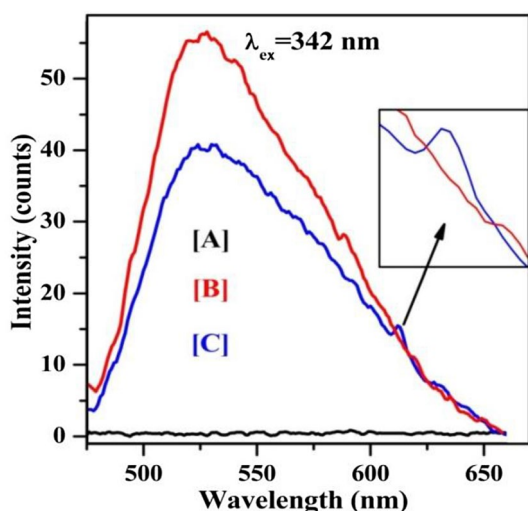


Fig. 6 Photoluminescence spectra of Eu:Y₂O₃ [A], YAG:Ce [B], and 3EY [C] on excitation with 342 nm wavelength. Inset: the enlarged portion of the photoluminescence spectra 3EY and YAG:Ce nanophosphor on 342 nm excitation

respectively (as shown in Fig. 5). When the 3EY was excited with 342 nm wavelength, a typical broad emission band corresponding to the Ce³⁺ ion was observed (Fig. 6).

While no any emission was observed in the same region in the case of Eu:Y₂O₃ nanophosphor on excitation with 342 nm, in the case of 3EY, along with the characteristic broad band corresponding to the Ce³⁺ ion emission, a slight intensified Eu³⁺ ion emission was also observed at 615 nm (see inset Fig. 6) overlying on the Ce³⁺ ion emission band. Additionally, the emission intensity of the Ce³⁺ band was

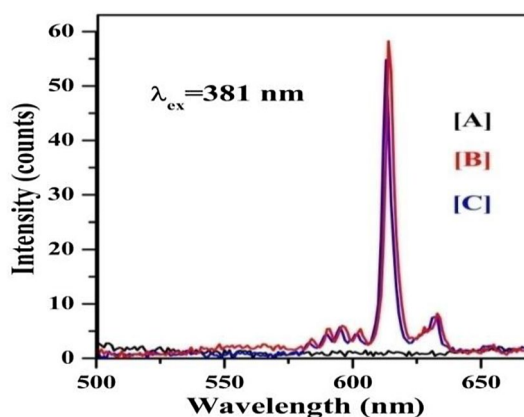


Fig. 7 Photoluminescence spectra of YAG:Ce [A], Eu:Y₂O₃ [B], and 3EY [C] nanophosphors on excitation with 381 nm wavelength

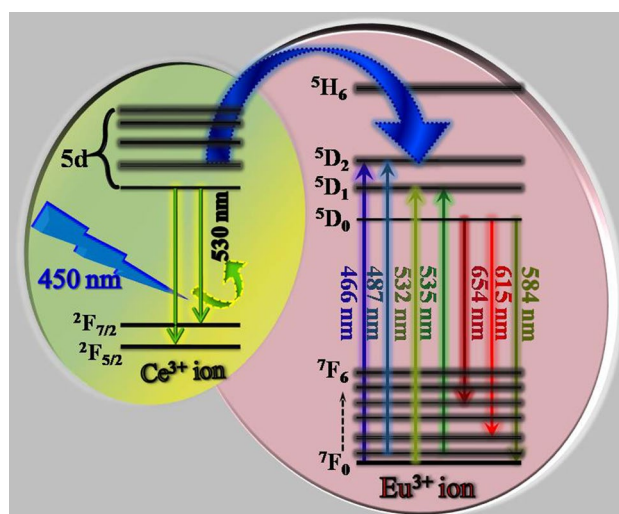


Fig. 8 Schematic diagram representing the energy transfer from Ce³⁺ to Eu³⁺ ion, in 3EY nanophosphor

found to reduce in comparison with YAG:Ce. The above observation speculates the interaction between the individuals of the 3EY and energy transfer form. Another narrow wavelength region, centered at 381 nm, corresponding to the excitation of Eu³⁺ ion exclusively excites only Eu³⁺ ion. The photoluminescence spectrum (see Fig. 7) reveals that on 381 nm excitation, only selective excitation of Eu³⁺ ions occurs, which leads characteristic emission profile of Eu³⁺ ion similar to the emission profile observed in the case of Eu:Y₂O₃.

However, no any band corresponding to the Ce³⁺ ion emission was observed indicating the occurrence of only one way energy transfer process, i.e., from Ce³⁺ → Eu³⁺ ion.

Nevertheless, the transfer from Eu³⁺ → Ce³⁺ cannot be established from the available data. Diagram representing the schematic of the energy transfer from Ce³⁺ → Eu³⁺ ion is depicted in Fig. 8.

3.5 Laser excitations

Photoluminescence spectra of synthesized samples using a combination of 405 nm and 450 nm wavelengths from cw laser diodes and CCD detector were monitored. The band positions in the emission spectra of 3EY and 6EY, YAG:Ce, and Eu:Y₂O₃ nanophosphors are identical to the spectra monitored using photoluminescence setup (Fig. 5).

3.5.1 405 nm excitation

When 3EY nanophosphor is excited with 405 nm (Fig. 9), YAG:Ce nanophosphor, Ce³⁺ ion gets partially excited due to their elongated excitation band edges.

On the other hand, Eu³⁺ ions get excited with 405 nm wavelength. When Eu:Y₂O₃ nanophosphor is excited with 405 nm, strong emission corresponding to the characteristic transitions between energy states of trivalent Eu³⁺ ion are observed. Similarly, when YAG:Ce nanophosphor was excited with 405 nm, a small intensity band centered at 511 nm and 560 nm was observed, which is corresponding to the 4*f*–5*d* transitions of Ce³⁺ ion. In the case of 3EY nanophosphor, it was observed that the emission bands got webbed over the entire spectrum range of 500–640 nm, composed of the combined emission yield by the Ce³⁺ and Eu³⁺ ions. However, a small increment in the overall emission intensity corresponding to Eu³⁺ ion transitions can be observed.

3.5.2 450 nm excitation

On excitation with 450 nm, Ce³⁺ ion gets resonantly excited; however, Eu³⁺ ion did not get excited. Eu:Y₂O₃

nanophosphor did not yield any emission due to the absence of excitation band at 450 nm (Fig. 10).

On the other hand, in the case of YAG:Ce nanophosphor, the characteristic emission profile of Ce³⁺ ion was observed on excitation with 450 nm. When 3EY nanophosphor was excited with 450 nm laser radiation, emission due to both Ce³⁺ ion as well as Eu³⁺ ion, were observed. The observation of Eu³⁺ ion emission is in-line with the result drawn from the excitation with 464 nm as explained above (see Fig. 5) and which establish the energy transfer from Ce³⁺ to Eu³⁺ ion.

3.5.3 Dual (405 nm + 450 nm)-beam excitation

To explore the consequences of the dual laser beam excitations (405 nm + 450 nm) (Fig. 11), PL experiments were performed, and a comparison between the PL spectra on exciting with 405 nm, 450 nm, and dual (405 nm + 450 nm) radiations were made.

In the case of Eu:Y₂O₃, typical 4*f* transitions emission peaks were observed on 405 nm excitation which was completely absent while exciting the same material with 450 nm. When samples were excited with dual (405 nm + 450 nm) radiations, no significant modification in the emission intensity was noticed for YAG:Ce and Eu:Y₂O₃ nanophosphors. The nanophosphor 3EY yields combinatorial emissions of both the ions with modified emission intensity. The emission intensity due to Ce³⁺ ion was found to be slightly reduced which in turn compensated to improve the emission intensity of the Eu³⁺ ion. The variation in the intensity of Eu³⁺ ion can be observed, indicating an efficient interaction between the two nanophosphors. To verify the concept of interaction among the doped species, the weight ratio (03:01 → 06:01) of Eu:Y₂O₃ was increased while keeping

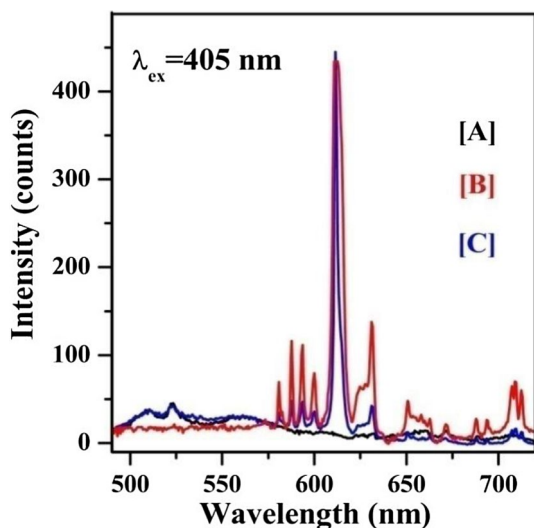


Fig. 9 Emission spectra of YAG:Ce [A], Eu:Y₂O₃ [B], and 3EY [C] nanophosphors on 405 nm excitation

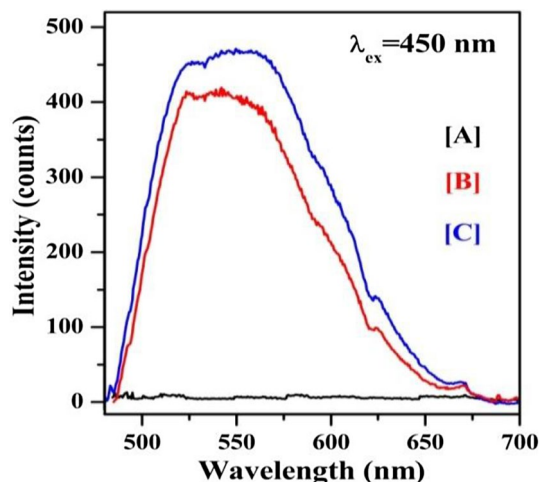


Fig. 10 Emission spectra of Eu:Y₂O₃ [A], YAG:Ce [B], and 3EY [C] nanophosphors on 450 nm excitation

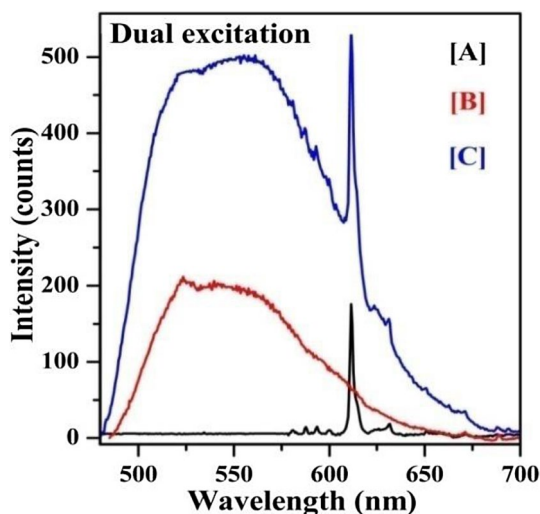


Fig. 11 Emission spectra of Eu:Y₂O₃ [A], YAG:Ce [B], and 3EY [C] nanophosphors on dual laser beam excitations (405 nm + 450 nm)

the YAG:Ce amount constant (Fig. 12). On excitation with 450 nm, a significant reduction in emission intensity of Ce³⁺ ion was observed, while the intensity of Eu³⁺ ion emission gets intensified, which was completely absent in 3EY. A close observation of the Ce³⁺ ion emission profile, in 6EY sample, reveals an obvious dip at 526 and 534 nm, which is in-line with the absorption of the Eu³⁺ ion at the same wavelengths. The observed dip affirms the concept of radiative energy transfer at least through Ce³⁺:4*f*-5*d* transition to Eu³⁺:⁷F_{0,1} → ⁵D₁ channel.

As a consequence of interaction among Eu³⁺ and Ce³⁺ ions, the overall color perception of emission change, hence

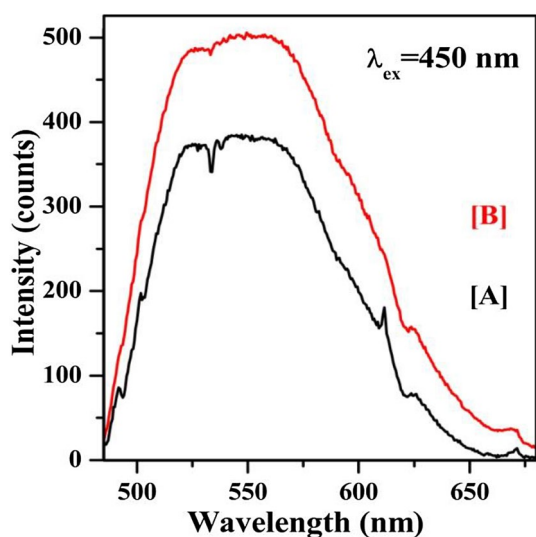


Fig. 12 Emission spectra of 3EY [A] and 6EY [B] nanophosphors on 450 nm wavelength excitation

color coordination, is expected to be significantly altered, which may be estimated by the CIE coordinates. The variation in the color perception of the combinational emissions can be characterized by the estimation of chromaticity coordinates (CIE-1931). CIE coordinates (*x*, *y*) on excitation with the wavelength 405 nm as well as 450 nm was estimated. The estimated CIE coordinate for Eu:Y₂O₃ nanophosphor lies at (0.44, 0.49) and (0.17, 0.27) [45] for YAG:Ce nanophosphor (0.34, 0.62) and (0.38, 0.57) [45, 46] and for the 3EY sample (0.39, 0.53) and (0.40, 0.53) corresponding to the excitation wavelengths 405 and 450 nm, respectively (Fig. 13).

The modification in CIE coordinates is expected due to the efficient interaction between both the ions. Variation in CIE coordinates, in the 3EY sample and YAG:Ce nanophosphor with the laser wavelengths 405 nm and 450 nm at different powers was monitored, and the noticeable variation was found. The coordinates obtained shifted as mentioned in Table 1. CCT as a function of varying laser power and CIE coordinates leading to the modification in overall color perception was calculated.

3.6 Decay curve analysis

To validate the concept of energy transfer (from Ce³⁺ to Eu³⁺ ions) as indicated by the photoluminescence analysis, the radiative lifetime was estimated by monitoring radiative decay curve of Ce³⁺ ions, at 530 nm emission, for specimens with YAG:Ce and Eu:Y₂O₃ in 3EY sample (see Fig. 14).

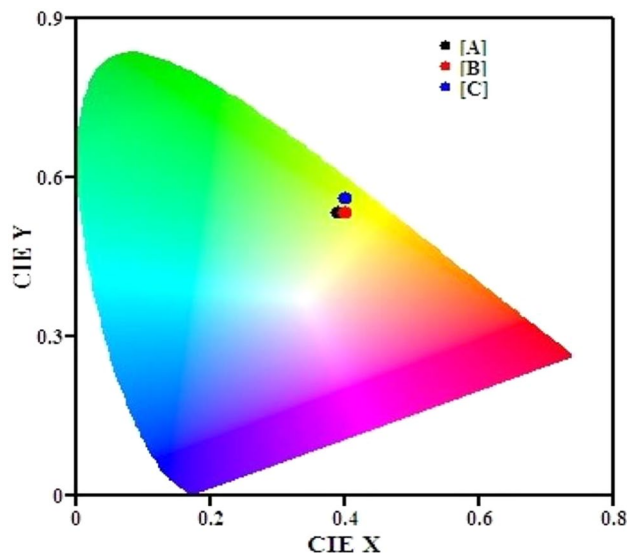
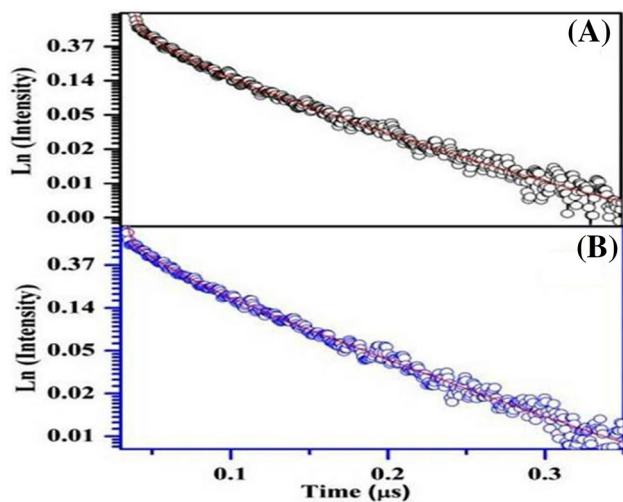


Fig. 13 CIE diagram containing the coordinates of 3EY sample on excitation with the laser of wavelength 405 nm [A], 450 nm [B], and dual (405 nm + 450 nm) [C]

Table 1 Calculated CIE coordinates and CCT of 3EY and YAG:Ce nanophosphors on excitation with 450 nm and 405 nm wavelengths

Excitation wavelength (nm)	Sample	Laser power (W)	CIE coordinates (x, y)	CCT (K)
450	3EY	0.74	(0.38, 0.57)	4722
		0.93	(0.38, 0.54)	4659
		1.13	(0.39, 0.56)	4545
		1.35	(0.39, 0.54)	4495
		1.50	(0.40, 0.53)	4306
	YAG:Ce	0.74	(0.37, 0.58)	4894
		0.93	(0.37, 0.57)	4879
		1.13	(0.37, 0.56)	4863
		1.35	(0.38, 0.57)	4722
		1.50	(0.38, 0.56)	4702
405	3EY	0.74	(0.32, 0.59)	5726
		0.93	(0.37, 0.55)	4846
		1.13	(0.38, 0.54)	4659
		1.35	(0.39, 0.54)	4495
		1.50	(0.39, 0.53)	4468
	YAG:Ce	1.50	(0.34, 0.62)	5395

**Fig. 14** Radiative decay curves of 3EY [A] and YAG:Ce [B] nanophosphors (excitation wavelength at 450 nm and emission at 530 nm wavelength)

The decay curves of the samples were monitored on excitation with 450 nm wavelength, and the obtained decay curves were exponentially fitted to estimate the radiative lifetime. In the case of YAG:Ce nanophosphor, the decay time for Ce³⁺ ions (emission at 530 nm) was estimated to be 36.6 ± 1 ns. On identical excitation with 450 nm, lifetimes of the Ce³⁺ ions was found to be slower by ~ 05 ns (32.3 ± 1 ns) in the case of 3EY sample indicating the energy stored in the Ce³⁺ ions, partially, bypassed via Eu³⁺ ion [47, 48]. These analyses are in-line with the conclusion drawn

by the photoluminescence measurements; hence, the energy transfer from Ce³⁺ to Eu³⁺ ions can be validated. However, the vice versa was not established from experiments.

4 Conclusions

A detailed study on the Eu:Y₂O₃/YAG:Ce nanophosphor was presented and the comparison between the nanophosphors was discussed. The structural characterization of synthesized nanophosphors have been made using various techniques including XRD, SEM, TEM etc., which indicates the formation of the nano-sized crystals in the range of 12–24 nm. The optical study reveals the efficient energy transfer from Ce³⁺ to Eu³⁺ ions. Due to the energy transfer photoluminescence, spectra contain green–yellow emission of Ce³⁺ ions, in addition to a sharp peak in the red region corresponding to the emission of Eu³⁺ ions, on excitation with 464 nm wavelength. The color perception of the composite nanophosphor is significantly modified due to the efficient interaction between the Ce³⁺ and Eu³⁺ ions. The overall emission from the sample, due to energy transfer, translating into white colour having CIE coordinates (0.40, 0.53) at high laser power.

Acknowledgements Authors would like to acknowledge the financial support from the project SB/FTP/PS-093/2013 from Science and Engineering Research Board (SERB-DST), New Delhi.

References

1. T. Tomiki, H. Akamine, M. Gushiken, Y. Kinjoh, M. Miyazato, T. Miyazato, N. Toyokawa, M. Hiraoka, N. Hirata, Y. Ganaha, Ce³⁺ centres in Y₃Al₅O₁₂ (YAG) single crystals. *J. Phys. Soc. Jpn.* **60**, 2437–2445 (1991)
2. Z. Xia, A. Meijerink, Ce³⁺-doped garnet phosphors: composition modification, luminescence properties and applications. *Chem. Soc. Rev.* **46**, 275–299 (2017)
3. S.H. Shionoya, W.M. Yen (eds.), *Phosphor Handbook* (CRC Press, Washington, 1999)
4. C.W.E. van Eijk, Inorganic-scintillator development. *Nucl. Instrum. Methods Phys. Res. A* **460**(1), 1–14 (2001)
5. M. Shur, R. Zukauskas, Solid-state lighting: toward superior illumination. *Proc. IEEE* **93**(10), 1691–1703 (2005)
6. J. Tous, K. Blazek, L. Pina, B. Sopko, High-resolution X-ray imaging CCD camera based on a thin scintillator screen. *Radiat. Meas.* **42**(4–5), 925–928 (2007)
7. W.J. Tropf, *Yttrium Aluminum Garnet (Y₃Al₅O₁₂)*, *Handbook of Optical Constants of Solids*, vol. III (Academic Press, San Diego, 1998), pp. 963–986
8. J. Dwivedi, P. Kumar, A. Kumar, S. Sudama, V.N. Singh, B.P. Singh, S.K. Dhawan, V. Shanker, A commercial approach for the fabrication of bulk and nanophosphors converted into highly efficient white LEDs. *RSC Adv.* **4**, 54936–54947 (2014)
9. J.M. Phillips, M.E. Coltrin, M.H. Crawford, A.J. Fischer, M.R. Krames, R. Mueller-Mach, G.O. Mueller, Y. Ohno, L.E.S. Rohwer, J.A. Simmons, J.Y. Tsao, Research challenges to ultra-efficient inorganic solid-state lighting. *Laser Photon. Rev.* **1**, 307–333 (2007)

10. M.M. Borlaf, R. Kubrin, V. Aseev, A.Y. Petrov, N. Nikonorov, T. Graule, Deep submicrometer YAG:Ce phosphor particles with high photoluminescent quantum yield prepared by flame spray synthesis. *J. Am. Ceram. Soc.* **100**, 3784–3793 (2017)
11. J. Ueda, S. Tanabe, T. Nakanishi, Analysis of Ce³⁺ luminescence quenching in solid solutions between Y₃Al₅O₁₂ and Y₃Ga₅O₁₂ by temperature dependence of photoconductivity measurement. *J. Appl. Phys.* **110**, 053102 (2011)
12. P. Schlotter, R. Schmidt, J. Schneider, Luminescence conversion of blue light emitting diodes. *Appl. Phys. A* **64**, 417–418 (1997)
13. H.S. Jang, Y.H. Won, D.Y. Jeon, Improvement of electroluminescent property of blue LED coated with highly luminescent yellow-emitting phosphors. *Appl. Phys. B* **95**(4), 715–720 (2009)
14. J.R. Jayaramaiah, B.N. Lakshminarasappa, B.M. Nagabhushana, Chemical luminescence studies of europium doped yttrium oxide nanophosphor. *Sens. Actuators B* **173**, 234–238 (2012)
15. G. Blasse, B. Grabmaier, *Luminescent Materials* (Springer, Berlin, 1994)
16. C.R. Ronda, Phosphors for lamps and displays: an applicational view. *J. Alloys Compd.* **225**, 534–538 (1995)
17. Y. Dwivedi, S.N. Thakur, S.B. Rai, Study of frequency up-conversion in Yb³⁺/Eu³⁺ by cooperative energy transfer in oxyfluoroborate glass matrix. *Appl. Phys. B Lasers Opt.* **89**, 45–51 (2007)
18. P.A. Tanner, L. Fu, L. Ning, B.M. Cheng, M.G. Brik, Soft synthesis and vacuum ultraviolet spectra of YAG:Ce³⁺ nanocrystals: reassignment of Ce³⁺ energy levels. *J. Phys. Condens. Matter* **19**, 216213 (2007)
19. R.R. Jacobs, W.F. Krupke, M.J. Weber, Measurement of excited-state-absorption loss for Ce³⁺ in Y₃Al₅O₁₂ and implications for tunable 5d→4f rare-earth lasers. *Appl. Phys. Lett.* **33**, 410 (1978)
20. X. Yan, W. Li, X. Wang, K. Sun, Facile Synthesis of Ce³⁺, Eu³⁺ co-doped YAG nanophosphor for white light-emitting diodes. *J. Electrochem. Soc.* **159**(2), 195–200 (2012)
21. R. Marin, M. Backa, N. Mazzucco, F. Enrichi, R. Fratini, A. Benedetti, P. Riello, Unexpected optical activity of cerium in Y₂O₃:Ce³⁺, Yb³⁺, Er³⁺ up and down-conversion system. *Daltan Trans.* **42**, 16837–16845 (2013)
22. T. Han, L. Peng, S. Cao, D. Zhu, M. Tu, J. Zhang, Preparation of a core-shell structured Al₂O₃/YAG:Ce phosphor by a spray drying method and formation mechanism. *Rare Met. Mater. Eng.* **43**, 2311–2315 (2014)
23. X.-L. Liu, P.-X. Zhu, Y.-F. Gao, R.-H. Jin, Synthesis of free-standing sub-10 nm Y₂O₃:Eu particles on silica nanowire matrix and amplified luminescence performance. *J. Mater. Chem. C* **1**, 477 (2013)
24. H.S. Yoo, W.B. Im, S.W. Kim, B.H. Kwon, D.Y. Jeon, Continuous nanocoating of Y₂O₃:Eu³⁺ phosphor shell on SiO₂ core particles and its photoluminescence properties. *J. Lumin.* **130**, 153–156 (2010)
25. J. Su, Q.L. Zhang, C.J. Gu, D.L. Sun, Z.B. Wang, H.L. Qiu, A.H. Wang, S.T. Yin, Preparation and characterization of Y₃Al₅O₁₂ (YAG) nanopowder by co-precipitation method. *Mater. Res. Bull.* **40**, 1279–1285 (2005)
26. Y. Rashmi, Dwivedi, White light color tuning ability of hybrid dibenzoylmethane/YAG:Ce nanophosphor. *Spectrochim. Acta A* **206**, 141–146 (2019)
27. M. Upasani, B. Butey, S.V. Moharil, Luminescence studies on lanthanide ions (Gd³⁺, Tb³⁺) doped YAG: Ce phosphors by combustion synthesis. *IOSR-JAP* **6**, 28–33 (2014)
28. A. Ghosh, P. Selvaraj, S. Sundaram, T.K. Mallick, The colour rendering index and correlated colour temperature of dye-sensitized solar cell for adaptive glazing application. *Sol. Energy* **163**, 537–544 (2018)
29. G. Ledoux, D. Amans, C. Dujardin, K. Masenelli-Varlot, Facile and rapid synthesis of highly luminescent nanoparticles via pulsed laser ablation in liquid. *Nanotechnology* **20**(44), 445605 (2009)
30. K. Zhang, Q.F. Liu, Q. Liu, Y. Shi, Y.B. Pan, Combinatorial optimization of (Y_xLu_{1-x-y})₃Al₅O₁₂:Ce_{3y} green-yellow phosphors. *J. Comb. Chem.* **12**, 453–457 (2010)
31. A. Emiraliev, A.G. Kocharov, R.V. Bakradze, U. Karimov, Z.I. Ahmetzhanov, The neutron diffraction redefinition of the coordinates of the atoms of oxygen in yttrio-aluminium garnet. *Kristallografiya* **21**, 112 (1976)
32. Z. Kong, L. Qian, S. Yun, S. Xiao-Bin, Z. Hong-Mei, P. Yu-Bai, Effect of defects on the luminescence and scintillation property of YLuAG:Ce phosphors obtained by different synthetic routes. *Acta Phys. Chim. Sin.* **27**(8), 2001–2008 (2011)
33. M. Jarzebski, M. Koscinski, T. Białopiotrowicz, Determining the size of nanoparticles in the example of magnetic iron oxide core-shell systems. *J. Phys. Conf. Ser.* **885**, 012007 (2017)
34. W.T. Carnall, G.L. Goodman, K. Rajnak, R.S. Rana, A systematic analysis of the spectra of the lanthanides doped into single crystal LaF₃. *J. Chem. Phys.* **99**(7), 3443–3457 (1989)
35. G. Blasse, A. Brill, Investigation of some Ce³⁺ activated phosphors. *J. Chem. Phys.* **47**(12), 5139–5145 (1976)
36. W.W. Holloway Jr., M. Kestigian, Optical properties of cerium-activated garnet crystals. *J. Opt. Soc. Am.* **59**, 60–63 (1969)
37. H.E. Hoefdraad, The charge-transfer absorption band of Eu³⁺ in oxides. *J. Solid State Chem.* **15**, 175–177 (1975)
38. L.N. Puntus, V.F. Zolin, V.A. Kudryashova, V.I. Tsaryuk, J. Legendziewicz, P. Gawryszewska, R. Szostak, Charge transfer bands in the Eu³⁺ luminescence excitation spectra of isomeric europium pyridine-dicarboxylates. *Phys. Solid State* **44**, 1440–1444 (2002)
39. Y. Dwivedi, S.C. Zilio, Infrared cascade and cooperative multicolor up-conversion emissions in Y8V2O17:Eu:Yb nanophosphors. *Opt. Express* **21**, 4717 (2013)
40. T. Verma, S. Agrawal, Luminescent properties of Eu³⁺ co-doped Y₂O₃:Dy³⁺ phosphors synthesized via ceramic route. *J. Mater. Sci. Mater. Electron.* **29**, 7832–7841 (2018)
41. P. Salas, A. Arredondo, E. De Rosa, J.A. Montoya, C. Angeles, R.A. Rodriguez, L.A. D-Torres, Low temperature synthesis and structural characterization of nanocrystalline YAG prepared by a modified sol-gel method. *Opt. Mater.* **27**, 1793–1799 (2005)
42. A.M. Hofmeister, K.R. Campbell, Infrared spectroscopy of yttrium aluminium, yttrium gallium, and yttrium iron garnets. *J. Appl. Phys.* **72**, 638–645 (1992)
43. A. Potdevin, N. Pradal, M.L. François, G. Chadeyron, D. Boyer, R. Mahiou, Microwave-induced combustion synthesis of luminescent aluminate powders. *Sinter. Methods Prod.* **39**, 189–212 (2012). (**Dr. Volodymyr Shatokha (Ed.)**)
44. J. Trajic, M.S. Rabasovic, S. Savic-Sevic, D. Sevic, B. Babic, M. Romcevic, J.L. Ristic-Djurovic, N. Paunovic, J. Krizan, N. Romcevic, Far-infrared spectra of dysprosium doped yttrium aluminum garnet nanopowder. *Infrared Phys. Technol.* **77**, 226–229 (2016)
45. A.C.P. Rocha, L.H.C. Andrade, S.M. Lima, A.M. Farias, A.C. Bento, M.L. Baesso, Y. Guyot, G. Boulon, Tunable color temperature of Ce³⁺/Eu^{2+,3+} co-doped low silica aluminosilicate glasses for white lighting. *Opt. Express* **20**(9), 10034–10041 (2012)
46. Y. Pan, M. Wu, Q. Su, Tailored photoluminescence of YAG:Ce phosphor through various methods. *J. Phys. Chem. Solids* **65**, 845–850 (2004)
47. Z. Wang, A. Meijerink, Dye-sensitized downconversion. *J. Phys. Chem. Lett.* **9**, 1522–1526 (2018)
48. G. Chen, J. Damasco, H. Qiu, W. Shao, T.Y. Ohulchanskyy, R.R. Valiev, X. Wu, G. Han, Y. Wang, C. Yang, H. Agren, P.N. Prasad, Cascaded upconversion in an organic dye-sensitized core/shell fluoride nanocrystal. *Nano Lett.* **15**, 7400–7407 (2015)

Publisher's Note Springer Nature remains neutral with regard to jurisdictional claims in published maps and institutional affiliations.